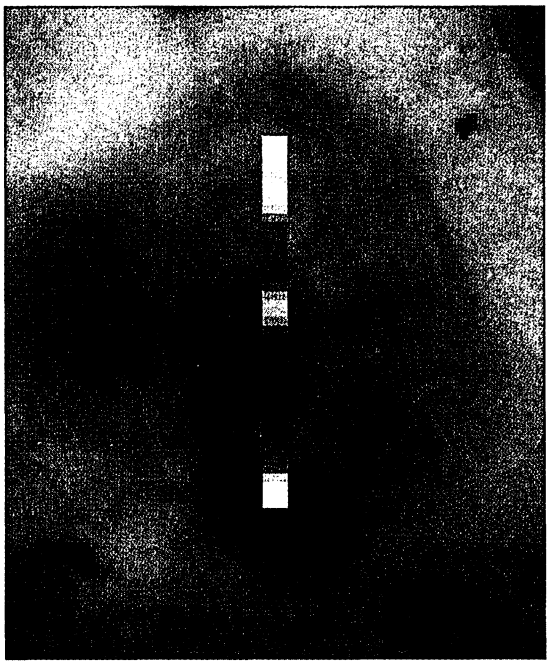

Fig. 4. NIMS obtained data over Culann Patera during the I25 flyby. A SO_2 relative band depth map (*9*) is shown over an SSI image acquired in July 1999. NIMS data show enhanced concentrations of SO_2 coinciding with deposits that are pink to red in visible wavelengths. Spatial resolution is 11 km/pixel (*22*), and the SSI image is 340 km across. The color scale is the same as in Fig. 3C.

S_2 solid nuclei on which SO_2 condenses. Alternatively, boiling liquid SO_2 with short-chain S or other coloring agents dissolved in it may reach the surface from below and freeze before complete sublimation. The diffuse appearance of the red deposits may arise from the entrainment of liquid droplets with escaping gases.

References and Notes

1. R. Lopes-Gautier *et al.*, *Icarus* **140**, 243 (1999).
2. R. W. Carlson *et al.*, *Geophys. Res. Lett.* **24**, 2479 (1997).
3. S. Douté *et al.*, in preparation.
4. P. E. Geissler *et al.*, *Icarus* **140**, 265 (1999).
5. R. G. Strom and N. M. Schneider, in *Satellites of Jupiter*, D. Morrison, Ed. (Univ. of Arizona Press, Tucson, AZ, 1982), pp. 598–633, and references therein.
6. Web fig. 1 is available at www.sciencemag.org/feature/data/1049493.shl
7. A. G. Davies *et al.*, *Lunar Planet. Sci.* **XXX** (1999) [CD-ROM].
8. The brightness temperature, T_B, is defined as $B(\lambda, T_B) = I(\lambda)$, where B is the Planck function, λ is the wavelength, and I is the corrected radiance. The corrected radiance is defined as $I(\lambda) = I_o(\lambda) - A * F(\lambda)$, where $I_o(\lambda)$ is the observed radiance, $F(\lambda)$ is incident solar flux at that wavelength, and A is an albedo estimate derived from the 1- to 2-μm region. For nightside observations, $I = I_o$. The color temperature, T_C, is defined as $B(\lambda_1, T_C)/B(\lambda_2, T_C) = I(\lambda_1)/I(\lambda_2)$. We used two pairs of (λ_1, λ_2): (4.1, 4.4 μm) and (4.4, 4.7 μm). The reported T_C is the average between the two values. In dayside observations, T_B and, in particular, T_C, are sensitive to the albedo used to correct the observed radiances, both in absolute value and its spectral slope (due to the SO_2 absorption at 4.1 μm). Therefore, calculations are made using a range of albedos, typically 60 to 80% of the value obtained at short wavelengths. The results are then averaged. Results displaying a high sensitivity to this variation (typically when $T_B < 200$ K) are omitted, as are those in which the error between the two estimates of T_C exceeds 20% of the mean. T_C is only calculated for pixels in which T_B exceeds a threshold (usually 210 to 250 K, depending on the noise level), to avoid errors due to the SO_2 absorption, since this absorption disappears at hot spots. Correct albedo values should yield $I(\lambda) = 0$ for the cold areas of Io. Small residual uncertainties in the NIMS calibration can sometimes yield a spurious $T_B \sim 180$ K for these areas, but pixels where $T_B < 200$ K were not used in this analysis.
9. The relative band depth is defined as the ratio [A(3.0)/A(4.1)], where A(λ) is the measured albedo (reflectance) at wavelength λ. This ratio was not obtained for pixels in which thermal emission could be detected.
10. B. Schmitt *et al.*, *Icarus* **111**, 79 (1994); B. Schmitt *et al.*, in *Solar System Ices*, B. Schmitt, C. De Bergh, M. Festou, Eds. (Kluwer Academic, Dordrecht, Netherlands, 1998), pp. 199–240.
11. We have checked and quantitatively calibrated this simple approach (segregated mixing and linear combination of computed radiances) by comparing the relative band depth map of a global observation taken in I24 with the SO_2 distribution maps of S. Douté *et al.* (*3*), which modeled 408-wavelength NIMS spectra.
12. J. R. Spencer *et al.*, *Science* **288**, 1208 (2000).
13. Times calculated using the model of A. G. Davies [*Icarus* **124**, 45 (1996)]. These temperatures and cooling rates assume that the surface heat loss is buffered by the release of latent heat from a still-molten flow interior.
14. R. Howell *et al.*, *Lunar Planet. Sci.* **XXXI** (2000) [CD-ROM].
15. A. S. McEwen *et al.*, *Science* **288**, 1193 (2000).
16. A. S. McEwen *et al.*, *Science* **281**, 87 (1998).
17. A. S. McEwen *et al.*, *Icarus* **135**, 181 (1998).
18. S. W. Kieffer *et al.*, *Science* **288**, 1204 (2000).
19. Previously undetected hot spots detected by NIMS during I24 and I25 are located at (+21, 146W, near Surya), (+14, 150 W), (+20, 149W), (+12, 158W, near Chaac), (–5, 132W, the dark feature Seth), and (+9, 133W)
20. J. C. Pearl and W. M. Sinton, in (*5*), pp. 724–755.
21. J. R. Spencer *et al.*, *Icarus* **127**, 221 (1997).
22. The pixel size in NIMS-processed images is 0.5× the instrument's spatial resolution.

23. Portions of this work were performed at the Jet Propulsion Laboratory, California Institute of Technology, under contract with NASA.

15 February 2000; accepted 18 April 2000

Prometheus: Io's Wandering Plume

Susan W. Kieffer[1]*, Rosaly Lopes-Gautier,[2] Alfred McEwen,[3] William Smythe,[2] Laszlo Keszthelyi,[3] Robert Carlson[2]

Unlike any volcanic behavior ever observed on Earth, the plume from Prometheus on Io has wandered 75 to 95 kilometers west over the last 20 years since it was first discovered by Voyager and more recently observed by Galileo. Despite the source motion, the geometric and optical properties of the plume have remained constant. We propose that this can be explained by vaporization of a sulfur dioxide and/or sulfur "snowfield" over which a lava flow is moving. Eruption of a boundary-layer slurry through a rootless conduit with sonic conditions at the intake of the melted snow can account for the constancy of plume properties.

Of the many remarkable phenomena on Io, one of the most intriguing is the wandering of some of the large plumes, the so-called "Prometheus-type plumes" (*1–3*). A new dark feature, interpreted to be a lava flow, connects the Voyager-era and Galileo-era plume sources. During the past 4 years, the lava has apparently been building up on top of itself rather than advancing farther west, because a large lava delta is the most pronounced feature on the west end, and the position of the plume within this area has not changed, nor have its geometric and optical properties. Material around, and presumably under, the lava flow consists of bright plains, which are interpreted to be a snowfield (*4*) of SO_2 and/or S. Such a steady, continuous discharge of material over such a long period of time is unlike that ever seen at terrestrial volcanoes.

It had been assumed by most researchers that the gas required to drive the plumes on Io

[1]S. W. Kieffer Science Consulting, Inc., 6 Queen Street, Suite 206, Post Office Box 520, Bolton, ON L7E 5T4, Canada. [2]Jet Propulsion Laboratory, California Institute of Technology, Pasadena, CA 91109, USA. [3]Lunar and Planetary Laboratory, University of Arizona, Tucson, AZ 85721, USA.

*To whom correspondence should be addressed. E-mail: skieffer@geyser.com

was released from stationary conduits, where magma or a sulfur, sulfur-dioxide, or magma mixture reaches the surface. However, migration of some plumes and the new high-resolution thermal and imaging data suggest the possibility that some of the plumes are disconnected from the location where the magma reaches the surface (*1*, *2*). Here we model a system for generating Prometheus-style wandering plumes.

The physical model. We postulate that the source of the Prometheus plume is a rootless conduit in the lava flow near the flow front (Fig. 1). Such conduits produce cones and craters on Earth, variously called pseudocraters, rootless cones, or littoral cones (*5*). These are best documented in Iceland and Hawaii (*6*–*9*). Rootless cones form by explosive interaction between molten lava and surface, or near-surface, water. Physical mixing of lava and water results in high rates of heat transfer, and the thermal energy of the lava is converted into mechanical energy of explosive vaporization (*10*, *11*).

Observations of the Prometheus lava flows indicate that they are between 1 and 100 m thick (*12*). We will assume 30 m for the thickness of the lava flow for our model. The ambient surface pressure on Io is $\sim 10^{-11}$ MPa, approximately the vapor pressure of SO_2 at 130 K. The ambient surface pressure increases if a lava flow covers the surface. For a 30-m thick flow, the basal pressure is ~0.1 MPa if the density is assumed to be ~2200 kg m^{-3} (*13*). The melting point of SO_2 at 0.1 MPa pressure is 266 K; for S, 393 K. Parameters required for the thermal modeling are density (ρ), heat capacity (*c*), thermal conductivity (*K*), and thermal diffusivity ($\kappa = K/\rho c$) for SO_2, S, and the lava (*14*).

A temperature-entropy (*T*-*S*) phase diagram (*15*, *16*) is useful for describing the thermal history of dynamic events such as that proposed here. We discuss SO_2 (Fig. 2) and S (Fig. 3) as the most probable dominant volatile phases in the snowfield. However, our conclusions should be qualitatively valid for other low-temperature volatile compounds, because we propose below that the major processes occur when the volatiles reach temperatures of several hundred kelvin, where most volatile compounds have their triple point temperatures.

Before being disrupted by the incursion of a lava flow, the snowfield is at the solid-vapor equilibrium point A, at 10^{-11} MPa (all references apply to both Figs. 2 and 3). The imposition of 0.1 MPa pressure on this snowfield by lava flow coverage would result in an excursion to the left to the 0.1 MPa isobar. If one assumes that the pressure remains constant during the heating, then the thermodynamic path will follow the 0.1 MPa isobar. Thickening of the lava flow by as much as an order of magnitude will not significantly change the conclusions because of the close proximity of the isobars on the *T*-*S* diagram.

As heating occurs over any given area near the surface of the snowfield, the volatile phases will remain solid until they reach temperatures at the triple point (path AB). With continued heating, the snowfield heats through the solid + liquid field (path BC). The volatiles will then further heat as a liquid (path CD) until they enter the liquid + vapor field (at point D). If the enthalpy of vaporization is available and if the snowfield material does not move (we show below that it probably does migrate at this point), the volatile phases can convert, partially or totally, to the vapor phase (path DE) and, after vaporization, will follow the 0.1 MPa isobar in the vapor field (path EF). The paths ABCDEF in Figs. 2 and 3 represent implicitly the time history of SO_2 or S near the interface with the lava flow.

Lava flow cooling and snowfield heating. In order to estimate the time scales for heating and cooling of the two materials, consider two models that bracket possible thermal interactions between lava and snowfields: a strictly conductive model and an advective (ablation-based) model that broadly accounts for massive fluid move-

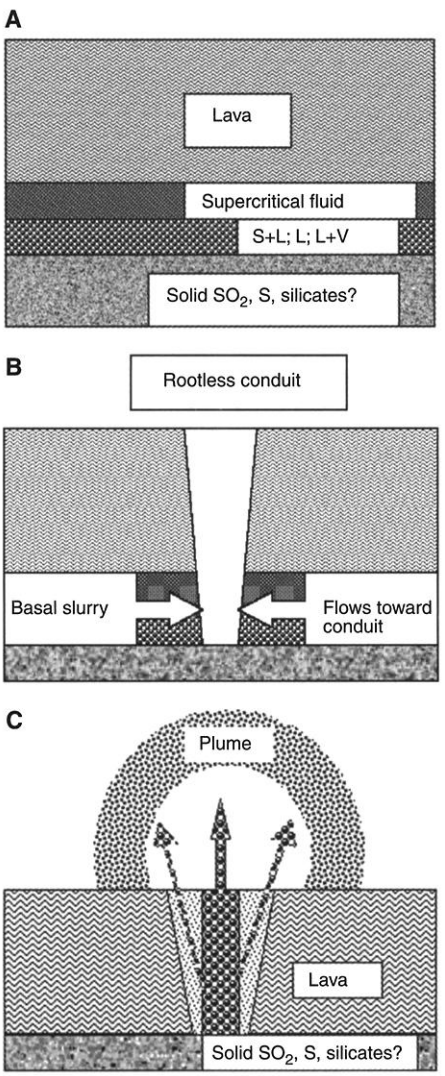

Fig. 1. Schematic illustration of the development of a Prometheus-style conduit and plume. S, solid phase; L, liquid; V, vapor. **(A)** Conditions within minutes after a lava flow covers a snowfield; see text for time and space scales. **(B)** Initiation of movement of boundary-layer slurry toward the conduit. **(C)** Steady state in which feeding of the conduit effectively keeps the base of the lava flow at the liquidus temperature of SO_2 or S. As the boundary-layer slurry rises in the conduit, it vaporizes and accelerates into the plume.

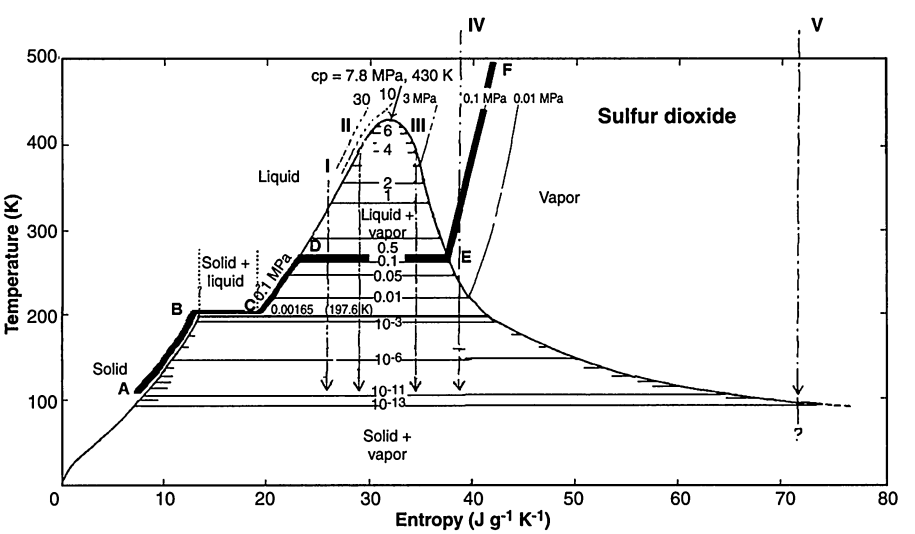

Fig. 2. Temperature-entropy phase diagram for SO_2, adapted from Smith *et al.* (*15*) Roman numerals I to V refer to possible volcanic eruption conditions described in Kieffer (*16*). In the solid region of the phase diagram, near point A, the isobars are so crowded together that they cannot be shown at this scale.

ment from the heated interface between the lava flow and the snowfield.

If all heat transport was by simple heat conduction, the lava and snowfield can be represented as infinite half spaces brought into contact at $t = 0$. One half-space represents the lava flow, assumed to be at 2000 K; the other half-space represents the snowfield at 130 K. The governing equations for this problem and its solutions are well known (*17*). The calculations show that SO_2 at ~10 cm depth can become a supercritical vapor (path ABCDE in Fig. 2) within ~80 min. Within 200 min, ~30 cm of the snowfield can be turned into liquid or vapor. On a longer time scale, if the heat transfer rate is constant, this melting rate is 785 m year^{-1}. The time scales would be somewhat longer for S, because the critical point is at much higher temperatures, but, as discussed below, we do not believe that the volatiles remain on the 0.1 MPa isobar once liquid conditions have been reached (266 K for SO_2 and 393 for S).

Meanwhile, at the base of the lava flow, a rigid crust forms at ~1450 K. Within 10 min, ~5 cm of crust has formed; within ~200 min, ~22 cm of crust has formed. Thus, the boundaries of the liquid + vapor field in SO_2 and the thickening crust grow nearly symmetrically with time.

According to this conductive model, the lava flow snowfield would develop a layered stratigraphy (Fig. 1A), consisting of hot, possibly supercritical fluid, as well as various mixtures of vapor, liquid, and solid phases. However, such a stratigraphy is highly unstable because of the buoyancy of the volatiles and the differential densities of the layers of liquid and vapor. The layers at the boundary would mix rapidly, producing a complex fluid mixture that we call the "boundary-layer slurry."

Given the instability of the crust over moving, tube-fed pahoehoe flows, a conduit inevitably opens to the surface, and the process becomes dynamic, rather than static, as modeled thus far. Once a conduit is formed, material from the boundary-layer slurry flows down the pressure gradient toward the conduit (Fig. 1B) to feed an eruption plume (Fig. 1C). In this lateral motion, removal of the boundary-layer slurry will expose colder and colder snowfield material to the lava flow. Erosion of any of the basal crust of the lava would also expose warmer lava continuously to the snowfield. We conclude that the melting and vaporization rates calculated above (~30 cm in 200 min or 785 m year^{-1}) represent minimum vaporization rates.

As an approximation to this very dynamic situation, consider a model in which any boundary-layer slurry formed is removed by lateral flow and eruption so rapidly that the interface between the snowfield and the base of the lava flow is kept at the liquidus temperature of the SO_2 (266 K), or S (393 K) (Fig. 1C). A solution to this problem is obtained by transforming the static coordinate system used in the conductive model above into a coordinate system on the (moving) snow-melt boundary that is working its way down into the snowfield at a velocity U (*14*, p. 292). U can be determined from the requirement that the flux, F, of heat flowing into the boundary from the lava flow is used to heat the snow up to melting temperature and to melt it

$$U = F/(H^*\rho) \quad (1)$$

The enthalpy, H, required to heat SO_2 from 130 K and to melt it totally at 197 K , is 195 J g^{-1}. The flux can be estimated from the assumed thermal conductivity and an assumed thermal gradient. Using the thermal conductivity model (22 cm of crust in 200 min) and a temperature gradient of 1600 − 266 = 1334 K, a basal thermal gradient of 6060 K m^{-1} is obtained. The basal flux F is then ~20×10^3 W m^{-2}. From Eq. 1, the calculated melting rate of the SO_2 ice to liquid would be 6.4×10^{-5} m s^{-1}, 5.5 m day^{-1}, or 2.0 km year^{-1}.

These models are simple extremes and include a number of assumptions, most of which suggest that these numbers represent upper limits on the vertical melting rate into the snowfield. Nevertheless, it seems reasonable to assume that vertical melting under the lava flow should be on the order of a kilometer per year.

Constancy of mass flux. The most challenging problem is to explain how the plume from Prometheus has maintained constant geometrical and optical properties, because this observation implies that the mass flux from the conduit must have remained constant over nearly 20 years. Mass flux through a circular cross section is given by

$$M = \rho^* u^* \pi r^{*2} \quad (2)$$

In this equation, ρ^*, u^*, and r^* are the density, vertical velocity, and radius, respectively, at the narrowest point of the conduit, typically the base, because acceleration of the flow tends to widen the conduit toward the top. Either all variables on the left side of the equation remain constant, or they must compensate in a way that keeps the mass flux, M, constant for 20 years. The simplest assumption is that each variable itself remains relatively constant as the lava flows along over the snowfield, a reasonable assumption for a very long lava flow. To justify this assumption, we analyze the dependence of each of the variables on planetary, lava, and boundary-layer slurry properties.

As the boundary-layer slurry accelerates from slow Darcy-like flow around the base of the conduit up the conduit and into the atmosphere, it passes through sonic and into supersonic conditions because of the large pressure gradient (~11 orders of magnitude) (*15*). A consequence of this condition is that flow properties are determined at the narrowest point in the conduit, denoted by * in Eq. 2. The flow velocity, u^*, will be equal to the sound speed, c^*, at the narrowest point in the conduit.

Conduit radius, r^*, is relatively constant because it depends strongly on parameters that do not change at all (planetary gravity), or change relatively little for long lava flows (yield strength, density contrast between the lava and the underlying flowing slurry, and—weakly in some cases—on flow thickness). In their classic 1981 paper (*18*), Wilson and Head demonstrated that there are two possible limiting constraints on the radii of conduits that permit magma to reach the surface [equation 20 and equation 24 in (*18*)]. In our model, the conduit radius is controlled by a

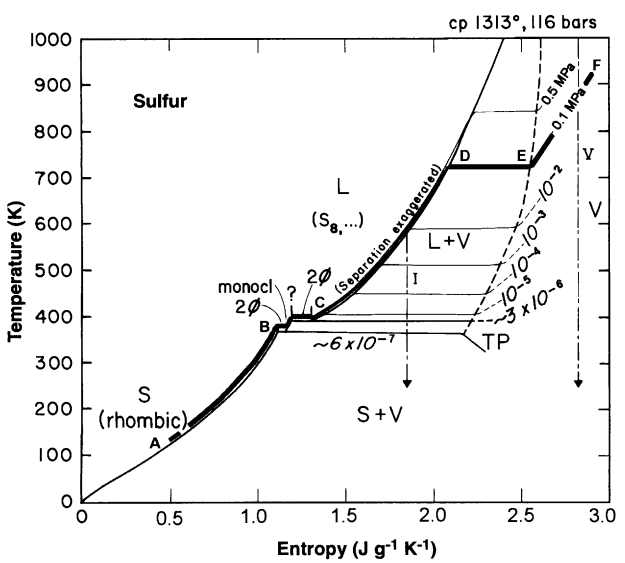

Fig. 3. Temperature-entropy phase diagram for S, adapted from Kieffer (*16*), with correction made to units on the entropy axis. Discussion of Fig. 2 applies.

constraint on the yield strength of the boundary-layer slurry [equation 20 in (*18*)] and depends only on a geometric constant, the yield strength, planetary gravity, and the differential density between the lava flow and the boundary-layer slurry. The radius is independent of the thickness of the lava flow, a fact that would work favorably toward keeping conduit radius constant as the flow travels long distances or as it forms a pond in the western delta.

The yield strength of a water-saturated slurry at the base of Antarctic ice streams, which may be the most relevant material to compare with our boundary-layer slurry, is ~1 to 5 × 10^3 N m^{-2} (*19*). We assume that the density of the boundary-layer slurry is close to the density of the SO_2 liquid, 1600 kg m^{-3}, because we are assuming that as soon as the liquid forms, it migrates toward the conduit. Although some vapor bubbles may form (see below), it is unlikely that there will be sufficient vaporization at the base of the conduit to cause a large density change. The results from equation 20 in (*18*) are shown in Table 1. Because this theory is an order-of-magnitude theory and because we expect conduit diameters on the "large" size on Io, we will take a conduit radius of 10 m for further calculations.

The next challenge is to demonstrate that ρ^* and $u^* = c^*$ will be relatively constant. As the liquid-dominated slurry moves toward the conduit, it will move into a lower-pressure environment. At some point along this migration path, bubbles of vapor will form. From the perspective of the *T-S* diagrams (Figs. 2 and 3), the fluid departs from the 0.1 MPa isobar toward lower pressures between points C and D (10^{-3} to 10^{-6} MPa for SO_2 and S, respectively). The lever rule, applied to any isobar, gives the vapor mass fraction, which is very small because the fluid is on the low-entropy side of the phase diagram (*15*). In this case, the density of the fluid remains close to the density of the liquid phase and it is appropriate to take $\rho^* \approx \rho \approx$ constant.

However, the compressibility of this liquid-bubble mixture is that of the nucleated vapor phase. This combination of high density with high compressibility leads to a fluid with very low sound speeds, c^*, typically ~10 m s^{-1}. If more vapor bubbles form, the density decreases, but the sound speed increases, and so there is a built-in compensatory effect in the product $\rho^* c^*$. Thus, with ρ^*, r^*, and $u^* = c^*$ all approximately constant, the mass flux from the eruption remains constant with time.

Systems controlled by sonic conditions such as these are called "choked systems," and they provide among the best physical conditions for maintaining constant mass fluxes. Therefore, under conditions that are not physically unrealistic, mass fluxes from a rootless conduit can remain constant even though the conduit position may change as the lava flow moves.

Table 1. Values of conduit radius for various slurry yield strengths by using equation 20 in (*18*).

Yield strength (N · m^{-2})	Radius (m)
1,000	1.85
5,000	9.3
10,000	18.5

For a conduit of radius 10 m, a boundary-layer slurry density of 1600 kg m^{-3}, and a sound speed of 10 m s^{-1}, the calculated mass flux through the conduit is ~5 × 10^6 kg s^{-1}, corresponding to a volume flux ~3 × 10^3 m^3 s^{-1}. These fluxes are in the middle range of common terrestrial eruption rates and are in line with estimates published from measurements of the plumes. Johnson and Soderblom (*20*) estimate that the mass flux from Prometheus is >4 × 10^6 kg s^{-1}; Wilson and Head (*21*) estimated a mass flux of 10^7 kg s^{-1} or volume flux of 7000 m^3 s^{-1}; James and Wilson later said that this may be an overestimate (*22*). Thus, our calculated values are in good agreement with those estimated from spacecraft observations.

The vaporizing snowfield within the area at the base of the conduit cannot, by itself, provide the required flux, because the sonic velocities (~10 m s^{-1}) are greater than the meltdown rate (~1 × 10^{-5} m s^{-1}). The mass flux per unit area out of the conduit is ~2 × 10^4 kg m^{-2} s^{-1}, whereas the melting supply rate is ~2 × 10^{-2} kg m^{-2} s^{-1}. This implies that the conduit must draw down from an additional area that is the ratio of these two numbers, of approximately 10^6 m^2 (1 km^2) corresponding to a circular area of 560-m radius.

Prometheus: Wandering or bound? Volcanoes named after legendary figures, as are the volcanoes on Io, may not always behave as their legendary counterparts—the Prometheus of legend was bound to a stake, whereas Prometheus on Io has not been bound by any physical or mythological constraints. Although we have never seen this type of behavior on Earth, our theory is consistent with a number of characteristics of cones and craters over rootless conduits on Earth (*6–9*). Major similarities are (i) association of rootless conduits with pahoehoe lava-flows fed by tubes; (ii) similar crater floor radii as can best be defined, including planetary scaling effects; and (iii) use of energy drawn from a magma rapidly transferring its heat to drive the volatiles into expansion (*10*, *11*).

Several significant differences that must be explained are as follows: (i) analogous eruptions on Earth typically do not have precisely balanced amounts of heat and volatiles, so that they are pulsating in nature, taking seconds to minutes to recharge one or the other of the resources; (ii) eruptions on Earth usually have clusters of cones and conduits instead of a single conduit; and (iii) eruptions on Earth do not continue for 20 years.

The first difference could be explained simply by lack of spacecraft observations on the time scales required to see pulsating recharge. Short periodic shutdowns cannot be ruled out from the few spacecraft observations available. These shutdowns would be accompanied by waxing and waning stages in which the sonic velocity constraints are released. It is possible that some information about this process is stored in the finite width of the ring deposits around Prometheus—that is, the distances between the proximal and distal deposits may contain information about velocity variations during the eruptions. However, long-term shutdowns of Prometheus are ruled out by the observations over the past 20 years.

The second difference between a presumed single conduit on Io and clusters of cones on Earth is more difficult to explain. On Earth, time-transgressive explosion centers are established, with each center remaining active as long as (i) the lava tubes are able to deliver fresh lava and (ii) enough water exists at the site of the interaction. Thus, although terrestrial conduits occur in clusters spatially, they form individually at different times. A single conduit will be stable as long as the supplies of magma and volatiles are available, and then the lava will move to a new location where water supplies are favorable, producing the time-transgressive behavior observed on earth. Although small excursions of the conduit at Prometheus cannot be ruled out, nor can the existence of smaller cones around the conduit, it appears that there are sufficient magma and volatiles around Prometheus to keep one conduit stable for years. This process may be facilitated by the fact that liquid SO_2 has a very low viscosity and could thus migrate in from relatively large distances.

From this model, we can outline some possibilities for the future of Prometheus. The plume can remain where it is for as long as the lava and melted snowfield supplies are maintained. It is possible that in 1979 the lava flow was at a higher elevation on the slopes of the caldera and has flowed downhill into a preexisting low topographic feature. In this case, Prometheus may remain where it is until the lava overflows this feature, as appears to have been the case for the past ~3 years, and then move on. On the other hand, the heat from the lava may create its own depression by melting down the snowfield. In this case, Prometheus may cease wandering and erupting when the base of the snowfield is reached and not reappear until lava has found a new snowfield. By its own thermodynamics, Prometheus the wanderer may become Prometheus bound.

References and Notes

1. A. McEwen *et al.*, *Science* **288**, 1193 (2000).
2. R. Lopes-Gautier *et al.*, *Science* **288**, 1201 (2000).
3. A. McEwen *et al.*, *Icarus* **135**, 181 (1998).
4. The term "snowfield" in the context of Io means a flat plains area of certain spectral properties (*1–3*), and implied composition of S, SO_2 and/or silicate pyroclastic fragments or bedrock matrix. Significant SO_3 and some other S-compounds can be ruled out as major components based on the spectral data in the literature.
5. Terminology: Historical terms are pseudocraters, littoral cones, and rootless craters. Because we do not discuss the crater landforms, and because the word "littoral" has strong implications of seawater involvement, we later introduce the term "rootless conduit" for our specific discussion.
6. R. V. Fisher, *Geol. Rundsch.* **57**, 837 (1968).
7. _____ and H.-U. Schmincke, *Pyroclastic Rocks* (Springer-Verlag, Berlin, 1984), pp. 263–264.
8. M. M. Morrissey and T. Thordarson, *Eos* **72**, 566 (1991).
9. Z. Jurado-Chichay, S. Rowland, G. Walker, *Bull. Volcanol.* **57**, 471 (1996).
10. K. Wohletz and R. McQueen, in *Explosive Volcanism: Inception, Evolution, and Hazards*, Studies in Geophysics (National Academy Press, Washington, DC, 1984), chap. 12.
11. K. Wohletz, *Bull. Volcanol.* **48**, 245 (1986).
12. If the lava flows in the western delta were thinner than 1 m, they could not produce the extensive sheet flows observed in the I24 and I27 SSI images (*1*). If they were much thicker than 100 m, shadowed scarps would be visible at the flow margins. Based on the interpretation that the Prometheus lavas are inflated pahoehoe (*1*), and observations of similar inflated flows in the same size range on Earth, we suggest that the thickness of warm lava in the Prometheus lava "delta" is likely to be a few tens of meters.
13. We have based the density estimate on the assumption that the observed high temperatures for the lava flows (*2*) indicate a lava of mafic, that is, relatively dense, composition.
14. The triple point of S depends on a number of phase changes and ranges from 368 to 393 K. For lava at 1600 K, we assume $\rho = 2000$ kg m^{-3}; $c = 1000$ J kg^{-1} K^{-1}; and $K = 3$ W m^{-1} K^{-1}. This gives $\kappa = 1.3 \times 10^{-6}$ m^2 s^{-1}. For SO_2 ice or liquid at 130 K, we assume $\rho = 1600$ kg m^{-3}; $c = 840$ J kg^{-1} K^{-1}; and $K = 3.5$ W m^{-1} K^{-1} (a value obtained from low-temperature water-ice). This gives $\kappa \sim 2.6 \times 10^{-6}$ m^2 s^{-1}. Latent heat released and absorbed can be ignored to the level of approximation here. Lava will release latent heat as it crystallizes; typical latent heats for magma crystallization are ~500 kJ kg^{-1}. Under the fortuitous conditions considered here, the latent heat supplied by crystallization of the lava is almost exactly equal to the heat required for melting of the snow and the terms cancel in the conservation equations [M. Necati Ozisik, *Boundary Value Problems of Heat Conduction* (Dover, New York, 1968)]. Thermal conductivity could be appreciably lower if the lava is porous, or if temperatures are extremely high, perhaps by an order of magnitude. Lower values of thermal conductivity would extend the time scales calculated here.
15. B. A. Smith, E. M. Shoemaker, S. W. Kieffer, A. F. Cook II, *Nature* **280**, 738 (1979).
16. S. W. Kieffer, in *Satellites of Jupiter*, D. Morrison, Ed. (Univ. of Arizona Press, Tucson, AZ, 1982), fig. 18.5, p. 17.
17. H. S. Carslaw and J. C. Jaeger, *Conduction of Heat in Solids* (Clarendon, Oxford, ed. 2, 1959), p. 88.
18. L. Wilson and J. Head, *J. Geophys. Res.* **86**, 2971 (1981).
19. B. Kamb, *J. Geophys. Res.* **6**, 16585 (1991).
20. T. V. Johnson and L. A. Soderblom, in *Satellites of Jupiter*, D. Morrison, Ed. (Univ. of Arizona Press, Tucson, AZ, 1982), chap. 17, p. 637.
21. L. Wilson and J. W. Head, *Lunar Planet. Sci.* **XII**, 1191 (1981).
22. M. R. James and L. Wilson, *Lunar Planet. Sci.* **XXIX**, 1349 (1998) [CD-ROM].

23. Portions of this work were performed at the Jet Propulsion Laboratory, California Institute of Technology, under contract with NASA. We also thank T. Johnson for pointing out that we had Prometheus bound if we had a mechanism to stop the motion of the plume.

28 February 2000; accepted 18 April 2000

Discovery of Gaseous S_2 in Io's Pele Plume

John R. Spencer,[1]* Kandis Lea Jessup,[2] Melissa A. McGrath,[3] Gilda E. Ballester,[2] Roger Yelle[4]

Spectroscopy of Io's Pele plume against Jupiter by the Hubble Space Telescope in October 1999 revealed absorption due to S_2 gas, with a column density of $1.0 \pm 0.2 \times 10^{16}$ per square centimeter, and probably also SO_2 gas with a column density of $7 \pm 3 \times 10^{16}$ per square centimeter. This SO_2/S_2 ratio (3 to 12) is expected from equilibration with silicate magmas near the quartz-fayalite-magnetite or wüstite-magnetite buffers. Condensed S_3 and S_4, probable coloring agents in Pele's red plume deposits, may form by polymerization of the S_2, which is unstable to ultraviolet photolysis. Diffuse red deposits near other Io volcanoes suggest that venting and polymerization of S_2 gas is a widespread feature of Io volcanism.

Io's plumes, discovered by Voyager in 1979, are the most dramatic expression of its active volcanism, and the 300-km-high Pele plume was by far the largest seen by Voyager (*1*). Galileo images have shown the Pele plume on only one occasion, in late 1996 (*2*). The plume was imaged by the Hubble Space Telescope (HST) at 257 to 291 nm, very faintly against dark sky in July 1995, and in extinction during transit of Io across Jupiter's disk in 1996 (*3*). In the transit images, the observed decrease in plume optical depth toward longer wavelengths was explained either by fine-grained dust scattering or SO_2 gas absorption; other gas species were not considered at that time. Subsequent transit and dark-sky imaging in July 1997 did not detect the plume, which was therefore less active then.

In October 1999 we observed the Pele plume with the HST (Table 1) to distinguish gas from dust extinction and to support observations by the Galileo spacecraft, which flew within 611 km of Io, and within 1300 km of the Pele plume vent, at 5:06 universal time (UT) (*4*) on 11 October. Images were taken with the Wide-Field Planetary Camera 2 (WFPC2) in the F255W, F336W, and F410M filters, with solar-weighted wavelength ranges of 257 to 291, 315 to 358, and 400 to 417 nm, respectively. Spectra were obtained during Jupiter transit with the Space Telescope Imaging Spectrograph (STIS), using its charge-coupled device (CCD) detector, its low-resolution 168- to 306-nm G230LB grating, and an effective slit size of 0.1×10 arc sec, giving 0.3-nm spectral resolution. The slit was stepped to five positions in 0.1–arc sec increments (relative to Io) perpendicular to its length, with an integration time of 255 s at each position and the expected location of the Pele vent placed within the central slit position.

The images taken against dark sky (Fig. 1) detected the Pele plume in the F255W and (probably) F336W filters, showing that the plume was active and had some dust component, because detectable Rayleigh scattering by gas alone is not expected at Io plume gas densities (*5*). The plume was conspicuous in the F255W image taken against Jupiter's disk, with an altitude of about 350 km, but was not seen in the F336W filter, confirming the wavelength dependence of the extinction (*3*). The plume was also invisible against Jupiter in 1.5-km/pixel resolution clear- filter (400 to 1000 nm) images taken on 11 October at 9:50 UT (*4*, *6*).

The STIS data were processed as follows. Near-Io spectra are contaminated by the spectrum of Io's disk owing to the finite STIS pixel size and the HST point-spread function. To correct for this and establish the continuum level for the spectra, we combined the five STIS long-slit spectra into an image cube and fit Io's location in the image plane with a blurred model disk (*7*). We used the model to determine the fraction of the spectrum in each pixel (after blurring) that was contributed by Io's disk, and removed this contribution using an average Io spectrum taken from the regions of Io furthest from the limb. Grating-scattered light becomes significant at wavelengths below 240 nm and dominates the signal below 210 nm. We determined the scattered light level in the 210- to 220-nm region by comparing the depth of solar Fraunhofer lines in the data to those in a solar spectrum (*8*), and subtracted the scattered light

[1]Lowell Observatory, 1400 West Mars Hill Road, Flagstaff, AZ 86001, USA. [2]University of Michigan, Space Research Laboratory, 2455 Hayward Street, Ann Arbor, MI 48109, USA. [3]Space Telescope Science Institute, 3700 San Martin Drive, Baltimore, MD 21218, USA. [4]Department of Physics and Astronomy, Northern Arizona University, Flagstaff AZ 86011, USA.

*To whom correspondence should be addressed. E-mail: spencer@lowell.edu